ChemElectroChem

Research Article
doi.org/10.1002/celc.202300235

Chemistry Europe
European Chemical Societies Publishing

www.chemelectrochem.org

Elucidating the Influence of Intercalated Anions in NiFe LDH on the Electrocatalytic Behavior of OER: A Kinetic Study

Maike Berger,[a] Ioana M. Popa,[a] Leila Negahdar,[b] Stefan Palkovits,[a] Bastian Kaufmann,[c] Moritz Pilaski,[c] Harry Hoster,[d] and Regina Palkovits*[a]

The oxygen evolution reaction (OER) as one half-cell reaction of electrochemical water splitting has a fundamental impact on water splitting efficiency and thus on the competitiveness of electrochemically generated hydrogen in the energy market. Nickel-iron layered double hydroxides (NiFe LDH) are among the most promising electrocatalysts for efficient OER under alkaline conditions. Despite intensive research, correlations of the material properties and the resulting kinetically limiting surface processes are poorly investigated. This work focuses on the kinetic behavior of NiFe LDH catalysts containing different anions in the basal spacing in alkaline OER. Steady-state Tafel plots, impedance measurements as well as reaction order plots were used to elucidate differences in the catalytic performance. All catalysts showed a dual Tafel behavior and fractional reaction orders. For kinetic modelling, the physisorbed hydrogen peroxide mechanism and Temkin adsorption model were adopted to fit experimental data. Our study showed that the intercalated anions affect the kinetics of rate determining steps. The hypophosphite intercalated LDH possessed the highest OER activity and the first step as rate determining. While for both carbonate and borate intercalated NiFe LDH, the second step proved to be rate determining in the low Tafel region, while the first step was found to be rate-limiting in the high Tafel region.

Introduction

In light of the rapid industrial, technological and scientific progress of the past century and the continuing population growth, the world's energy demand continues to rise.[1] While the combustion of fossil fuels is not sustainable because of the associated greenhouse gas emissions, significant efforts have been made to develop green energy sources. To deliver continuous power through wind or solar energy, large scale energy storage is required, where renewable energy can be efficiently converted into storable species.[2] Central to this discussion is the use of green hydrogen as an efficient and clean energy carrier. The imperative need for green hydrogen has made the electrochemical water splitting more relevant than ever. In water splitting, the standard potential of 1.23 V is determined by the oxygen evolution side. However, kinetic inhibition of the OER due to sluggish kinetics and a complex mechanism increases the technically required potential and the so called overpotential (OP) must be exceeded to start the reaction. In order to make this process industrially competitive, affordable catalysts with good performances are currently being researched.[3,4] Among them, NiFe layered double hydroxides are of particular interest, as their low cost and abundancy offers an economic benefit, and simple interlamellar anion exchange can drastically improve their activity.[3] Due to their promising catalytic activity in alkaline OER and their versatile adjustment opportunities, extensive research has been carried out targeting improved activity and durability. Lu *et al.* found that, grown onto Ni foam, NiFe LDH only required an overpotential of ~280 mV to reach 30 mA cm^{-2} (η_{30}), which is even lower compared to an 20 wt% Ir/C catalyst with η_{30} of ~390 mV.[5] Stability measurements at 1.5 V applied voltage allowed a stable current density (~200 mA cm^{-2}) with only 2.2% degradation after 10 h, revealing very good stability under OER conditions. To increase conductivity, Zhang *et al.* alternately stacked NiFe LDH with CNTs to form an intercalating heterostructure of NiFe LDH/CNTs. Their catalyst only needed an overpotential of 234 mV to reach a current density of 10 mA cm^{-2} which was attributed to the synergy between active NiFe LDH and conductive CNTs.[6]

Carrasco *et al.* established a correlation between interlayer space and overpotential by intercalating surfactant sulfates as interlayered anions, exhibiting different chain lengths.[7] They

[a] M. Berger, I. M. Popa, Dr. S. Palkovits, Prof. Dr. R. Palkovits
Institute of Technical and Macromolecular Chemistry
RWTH Aachen University
Aachen 52074 (Germany)
E-mail: palkovits@itmc.rwth-aachen.de
Homepage: https://www.itmc.rwth-aachen.de/
[b] Dr. L. Negahdar
School of Chemistry
University College Dublin
D04 N2E5 Dublin (Ireland)
[c] B. Kaufmann, Dr. M. Pilaski
Zentrum für BrennstoffzellenTechnik GmbH
Duisburg 47057 (Germany)
[d] Prof. Dr. H. Hoster
Chair of Energy Technology
University of Duisburg-Essen
Duisburg 47048 (Germany)

Supporting information for this article is available on the WWW under https://doi.org/10.1002/celc.202300235

found that increasing the interlayer space from 11 Å to 25 Å led to enhanced activity with the overpotential η_{10} decreasing from 356 mV (NiFe-SO_4) to 316 mV (NiFe-DS). While these studies mainly focused on achieving superior catalysts performance, little effort has been made to gain a deeper understanding of why these particular performances occur. Indeed, it is fundamental to understand the influence of material properties on the mechanism in OER to enable a knowledge based catalyst design.[8] In addition, elucidating governing mechanisms and identifying kinetic bottlenecks allows for a better process design and operation control.[9,10]

Over the past decades, few studies have targeted a comprehensive mechanistical analysis of alkaline OER on metal oxide films.[10–13,14] Doyle *et al.* studied OER over iron oxyhydroxide films in alkaline solution. They proposed a mechanistic scheme that involves the active participation of octahedrally coordinated anionic iron oxyhydroxide surfaquo complexes, forming a porous hydrous layer. These layers were presumed to facilitate hydroxide ion discharge at the metal site during OER.[10] Scarr *et al.* studied OER on nickel and other metals and found that for nickel and its alloys, a dual Tafel behavior appeared.[15] Interpreting the obtained Tafel values, a mechanism involving a three-step formation of adsorbed hydrogen peroxide was proposed. The dual character suggested different rate determining steps in the adsorbed hydrogen-peroxide mechanism depending on the potential region. In our recent research, oxygen evolution was investigated over structured and non-structured Ni–Co oxides.[8] For the unstructured oxide, the obtained values for Tafel slope and reaction order suggested adsorption under Langmuir conditions, whereas the values for structured oxide implied Temkin adsorption conditions. Based on these findings, it was proposed that depending on the structural properties, differences in the strength of surface intermediates adsorption shift the rate limiting step. For OER, different possible mechanisms in acid and alkaline solution were proposed in literature.[15–17] In 1986, Masumoto *et al.* summarized different possible anodic OER mechanisms in alkaline media based on the work of Scarr *et al.*, Yaeger *et al.* and Brockis *et al.* (Table 1).[16]

Table 1. Possible mechanisms for the oxygen evolution reaction in alkaline media.

Electrochemical oxide path[18]	Oxide path[18]
$OH^- + M \rightarrow MOH + e^-$ $MOH + OH^- \rightarrow MO + H_2O + e^-$ $2\,MO \rightarrow O_2 + 2\,M$	$M + OH^- \rightarrow MOH + e^-$ $2\,MOH \rightarrow MO + M + H_2O$ $2\,MO \rightarrow 2\,M + O_2$
Krasil'shchikov path[15]	Yaeger's path[16]
$M + OH^- \rightarrow MOH + e^-$ $MOH + OH^- \rightarrow MO^{-+}H_2O$ $MO^- \rightarrow MO + e^-$ $2\,MO \rightarrow 2\,M + O_2$	$M + OH^- \rightarrow MOH + e^-$ $M^zOH \rightarrow M^{z+1}OH + e^-$ $2\,M^{z+1}OH + 2\,OH^- \rightarrow 2\,H_2O + O_2$
Bockris Path[17]	
$M + OH^- \rightarrow M\text{-}OH + e^-$ $M\text{-}OH + OH^- \rightarrow M\text{-}H_2O_2 + e^-$ $M\text{-}H_2O_2 + OH^- \rightarrow M\text{-}HO_2^- + H_2O$ $M\text{-}H_2O_2 + M\text{-}HO_2^- \rightarrow O_2 + H_2O + OH^-$	

Among these one-electron transfer reactions, the slowest one presents the rate determining step (RDS), and identifying it allows for an easier description of the overall rate of the anodic reaction. Based on the work of Masumoto *et al.*, two factors that mainly determine electrocatalysis efficiency of OER are the bond strength of MO in the adsorbed intermediate states (MO, MO^-, M- OH, M-H_2O_2, M-HO_2^-) and the electron transfer rate according to the *Franck-Condon* principle.[16]

Here, we present a comprehensive mechanistic investigation of the influence of anion exchange in NiFe LDHs on reaction mechanism and RDS, respectively. Beyond cyclic voltammetry, techniques such as elemental analysis, X-ray diffraction, impedance spectroscopy and steady-state polarization are used for characterizing the physicochemical and electrochemical material properties. Steady state operations open up the possibility to select the proper mechanism and adsorption model for calculating the RDS. Key kinetic parameters are determined and analyzed to explain the difference in behavior induced by anion exchange at otherwise constant catalytic conditions.

Results and Discussion

NiFe LDHs with a Ni/Fe ratio of 0.5 with carbonate, hypophosphite or borate (NiFeC LDH, NiFeP LDH and NiFeB LDH) as intercalated anions were prepared *via* co-precipitation starting from the metal nitrates based on the work of Luo *et al.*[19]

Prior to electrochemical activity studies, EDX and double-layer capacitance measurements were carried out to characterize metal content and electrochemical surface area (Figure 1). EDX analyses confirmed a comparable Ni/Fe ratio of the three catalysts with a slightly smaller Ni content for NiFeP LDH. The determined electrochemical surface areas were comparable with a slightly higher value for NiFeC LDH. Overall, the materials possess comparable characteristics allowing further analysis regarding the influence of interlayer anions on the electrocatalytic behavior in OER.

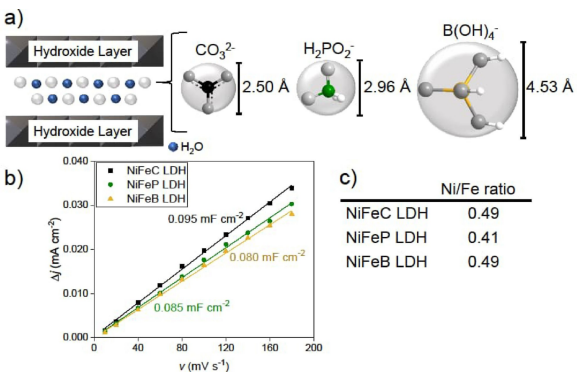

Figure 1. a) Schematic LDH structure with the intercalated anion carbonate, hypophosphite or borate and their respective anion diameter. b) Differences in charging current density Δj plotted against the scan rate under anodic potential. The linear fitting slope, approximating twice the double-layer capacitance C_{dl}, was used to represent ECSA. c) Ni/Fe ratio determined by EDX measurements.

XRD spectra (Figure 2) of all candidates show the characteristic two reflections for LDH (depicted as blue lines) which indicates a rhombohedral LDH structure and the (003) and (006) crystal planes in the LDH.[20,21] Since the intercalated anions in this experiment do not contain atoms with large scattering power, nickel and iron cations in the host layers are mainly responsible for the basal (00/) reflections.[20] The 2θ values for the (003) reflections are observed in the interval 10°–12° and indicate the varying basal spacing. From Bragg's law, it follows that the basal spacing increases as the (003) reflection shifts to lower 2θ values. In this case, changing the intercalated anion from carbonate to hypophosphite to borate resulted in a basal spacing increase from 7.5 Å to 7.75 Å to 10.16 Å, which is in good agreement with the increase in anion size visualized in Figure 1a. Besides the characteristic (003) and (006) reflections, two more peaks are observed around 35° and 62°. These can be attributed to the (012) and (110) reflections, respectively and further indicate the formation of two-dimensional LDH.[22] For NiFeC LDH additional reflexes exist which can be allocated to the formation of Fe_3O_4. Since it is known from literature that Fe_3O_4 has a weak activity in OER catalysis, the activity impact can be assigned to the LDH species.[23]

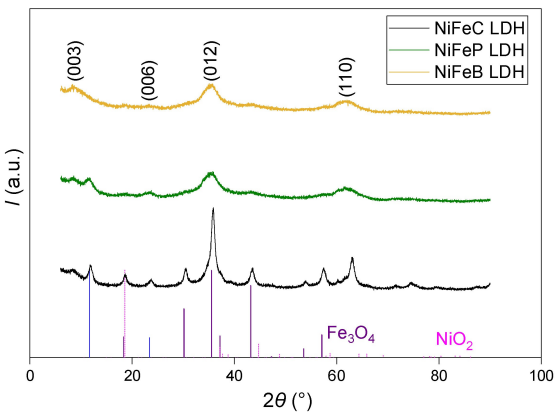

Figure 2. XRD spectra of NiFeC LDH (black), NiFeP LDH (green) and NiFeB LDH (yellow). Values were collected under CuK_α radiation ($\lambda = 1.54$ Å) with 2θ ranging from 6° to 90° in 0.02° steps. Reference lines for Fe_3O_4 (violet, ICSD #35000), NiO_2 (pink, ICSD #78698) and the characteristic (003) and (006) Peaks for LDH (blue, ICSD #107625) are marked. NiO_2 was not formed during synthesis.

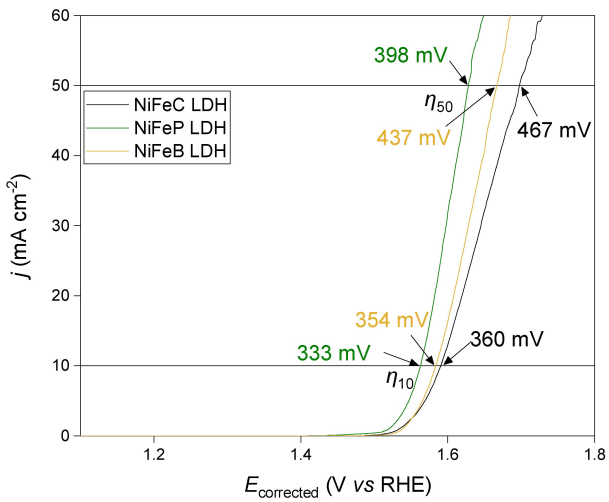

Figure 3. Polarization curves of NiFeC LDH (black), NiFeP LDH (green) and NiFeB LDH (yellow) vs the RHE potential scale for the OER. The data was collected at a scan rate of 5 mV s^{-1} using a three-electrode set-up with glassy carbon as the counter electrode (CE) and Ag/AgCl as the reference electrode (RE) in 1 M KOH as electrolyte without stirring. All curves are *iR* corrected.

OER performances of the catalysts were investigated by linear sweep voltammetry (LSV) on a rotating disk electrode (RDE) in a classical three electrode configuration and at a scan rate of 5 mV s^{-1} (Figure 3). Rotation of the RDE led to decreased activity which can be attributed to abrasion of the coating (Figure S1). Measurements were therefore performed without stirring. The LSV values were *iR* corrected in order to compensate for the electrolyte resistance, which was determined by impedance spectroscopy (Figure 7a).

The LSV curves emphasize that the overpotential at 10 mA cm^{-2} (η_{10}) decreases in the following order: Carbonate > borate > hypophosphite intercalated NiFe LDH from 360 to 354 to 333 mV, respectively. The overall trend becomes even more pronounced for higher currents densities with a difference of 69 mV at η_{50}.

The observed trend is in good agreement with literature, where different studies described the positive influence of substituting carbonate with hypophosphite on increased current density at constant potential.[18,19]

As origin of improved activity, the authors named the enlarged anion size and an correspondingly expanded basal spacing to be responsible for better accessibility of the active sites.[19,24] Another decisive difference of the anions relates to the redox behavior of hypophosphite. Hypophosphite is a stronger reducing agent which helps to maintain the active metal sites in lower valence states and allows for an easier electron transfer to the active sites. Metal sites in initially low valence states are advantageous as they are more easily oxidized during OER, so the high valence sites are more favored throughout the reaction and a better performance is expected.[19,25] The influence of borate is more challenging to explain. As confirmed by XRD analysis (Figure 2), NiFeB LDH exhibits the largest basal spacing caused by the bigger anionic radius which should positively influence activity. Although NiFeB LDH indeed performed better than NiFeC LDH, the borate intercalated LDH could not reach the activity of NiFeP LDH. We suggest that the observed trend is caused by two opposing effects. The increase of activity is caused by the bigger basal spacing whereas borate exhibits a less pronounced reducing character. This affects the activity negatively, since boron compounds suffer from an electron deficit which results in a less pronounced electron-donating character.

Since the activity trend is not comprehensively explained by only activity measurements, a need for mechanistical insight becomes evident. Therefore, steady-state Tafel plots were obtained from steady-state LSV curves. For all three catalysts, a change in Tafel slope was observed at approx. 360 mV overpotential. Tafel slopes of 72 mV dec^{-1}, 69 mV dec^{-1} and 60 mV dec^{-1} were observed in the low Tafel region for NiFeC, NiFeP and NiFeB, respectively, whereas values of 196 mV dec^{-1},

186 mV dec^{-1} and 148 mV dec^{-1} were observed in the high overpotential region. The increase in Tafel slope could be attributed to gas evolution which reduces the effectiveness of the electrodes surface. However, the agreement between the three curves supports the assumption, that the dual Tafel behavior is not due to experimental artefacts but can be attributed to a dual mechanistical behavior.[10,12] Indeed, we suggest that these changes are mostly assigned to a change in the RDS.[8] First, the noticeably higher Tafel slopes for NiFeC LDH in both regions underline again the lowest performance among the three catalysts. The overall lower Tafel slopes for NiFeB LDH would imply the best performance. This seemingly contradictory observation compared to CV data will be discussed later.

A further important parameter in discussing the Tafel plots is the transfer coefficient α, which is defined by Equation (1).[26,27] The first part of the equation once again highlights the relationship between the Tafel slope and the electrocatalytic performance: Since α is inversely proportional to the slope, a small slope correlates to a high activity and *vice versa*.[8] The second part of the equation allows for more mechanistical insight. Hereby, n_f refers to the number of electrons exchanged by the electrode before the RDS, $\upsilon$is the number of occurrences of the RDS in the assumed mechanism, n_r is the number of electrons involved in the RDS and β presents a symmetry factor.[27]

$$\alpha = \frac{1}{b}\left(\frac{2.303\ RT}{F}\right) = \frac{n_f}{\upsilon} + n_r\beta \tag{1}$$

When considering elementary steps in a mechanism, the simultaneous exchange of at most one electron is considered probable. When the RDS is a chemical step, that means that no electrons are involved, n_r will be 0. In the case of an electron transfer RDS, $n_r = 1$.[28] Another note to be made is that the symmetry factor β corresponds to the transfer coefficient for a one-electron transfer step and, for a symmetric potential energy barrier, is equal to 0.5. Deviations from this value will be discussed in the following interpretation.[27]

A generally accepted and plausible model for OER on nickel depicts the physisorbed hydrogen peroxide mechanism (Brockis Path, Table 1) and was used for modelling the kinetics in this experiment.[15,29] Considering every step as rate limiting, the Tafel slopes were calculated using Equation (1) (see Table S1). All calculated Tafel slopes did not agree with the observed values in Figure 4, so it follows that the assumption about the symmetry factor β is wrong. While there is no general agreement on the physical meaning of β, it is known that its value is close to 0.5 when describing a symmetric potential energy barrier.[30] The observed deviation from this value is not surprising, since the electron exchange with the metal active sites takes place when the reactant is in an adsorbed state. In this case, the adsorbed molecules bring their center of charge close to the electrode surface, at a distance smaller than the thickness of the Helmholtz double layer. Hence, the potential distance profile loses its symmetry, and β deviates from 0.5.[27] In order to properly assign a value toβ, the electrochemical

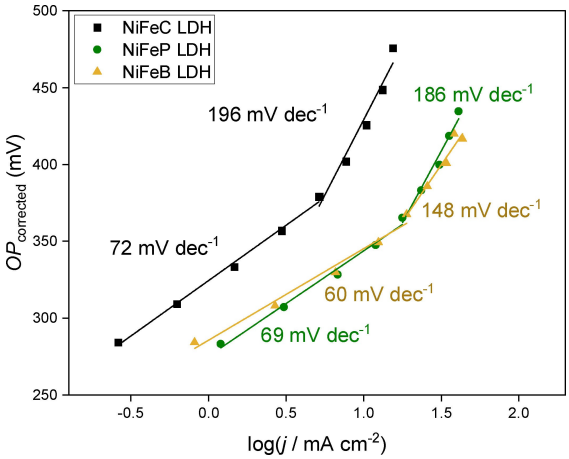

Figure 4. Steady-state derived Tafel plots (black: NiFeC LDH, green: NiFeP LDH and yellow: NiFeB LDH). Steady-state data was measured at nine different potentials from 0.5 to 0.7 V *vs* Ag/AgCl without stirring. For each applied potential, the current response was measured over 150 s and the last 25 data points were averaged.

reaction order $m_{X,V}$ of the hydroxyl anions must be analyzed. Here, a_X denotes the activity of the considered species X and V is the potential.[8]

$$m_{X,V} = \left(\frac{\partial \log i}{\partial \log a_X}\right)_V \tag{2}$$

The reaction order is strongly connected to the isotherm adsorption conditions of the reactants and intermediates at the electrode interface and may offer further insight into mechanistical aspects.[8] Calculated according to Equation (2), the reaction order has been investigated at the two potentials 0.575 V and 0.750 V (*vs* Ag/AgCl) which were selected as they represent the midpoint of the low (0.575 V) and the high (0.750 V) linear Tafel region. Figure 5 summarizes the results.

For kinetic studies, a mechanism consisting of elemental electron transfer or chemical reactions with a single RDS is assumed. In this case, only the elementary steps preceding and including the RDS affect the electrode kinetics, while all RDS subsequent steps can be ignored. Assuming Langmuir adsorption conditions, the first reaction step would likely not be rate-determining, as the adsorption under Langmuir conditions is strong and interactions between adsorbed gas molecules are negligible. Therefore, the second step is considered to be rate limiting and its flux is given by Equation (3).

$$f_T = f_2 = k_2^{'0}\ \theta_{MOH}\ a_{OH}\ \exp\left[\frac{\beta\ F\eta}{RT}\right] \tag{3}$$

According to the quasi-equilibrium approximation, the reaction rates of the forward and reverse reaction can be set as equal, which then results in Equation (4). At low surface coverage θ_{MOH}, the coverage of the metal sites θ_M can be seen as quasi-constant and the term can be substituted, resulting in Equation (5).

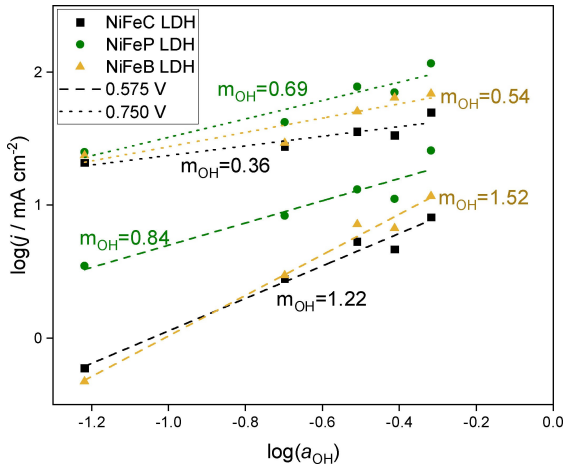

Figure 5. Reaction orders for the hydroxyl anions at 0.575 V and 0.750 V respectively (black: NiFeC LDH, green: NiFeP LDH, yellow: NiFeB LDH). The LSV data was collected at a scan rate of 5 mV s^{-1} using a three-electrode set-up with glassy carbon as counter and the Ag/AgCl electrode as reference electrode in KOH as electrolyte without stirring. Five different KOH concentrations were used in turn: 0.2, 0.4, 0.6, 0.8 and 1 M.

$$\frac{\theta_{MOH}}{\theta_M} = K_1\, a_{OH} \exp\left[\frac{F\eta}{RT}\right] \tag{4}$$

$$f_T = K_1\, k_2^{'0}\, \theta_M\, a_{OH}^2 \exp\left[\frac{(1+\beta)F\eta}{RT}\right] \tag{5}$$

According to Equation (2), a reaction order of 2 follows for the hydroxyl anions. In a similar manner, when analyzing the other elementary steps as possible RDS, integers will be obtained for the electrochemical reaction order of OH^-. These values do not fit to the experimental data, as mostly fractional reaction orders were obtained. This circumstance calls for using another hypothesis as the adsorption isotherm. In the case of Temkin adsorption conditions, more than one simultaneously adsorbed species is considered, which is the case when the adsorption is weak or competing mechanisms are present. As such, a fractional reaction order follows.[31]

In general, the heat of adsorption of reaction intermediates decreases linearly with the total coverage as a result of the repulsive interactions between the adsorbate molecules. In this case, we assume a coverage between 0.2 and 0.8 and the fluxes for the first reaction can be adjusted by adding a term which refers to the change in adsorption free enthalpy as follows:[12,32]

$$f_1 = k_1^{'0}\, \theta_M\, a_{OH} \exp\left[\frac{\beta F\eta}{RT}\right] \exp\left[\frac{-\gamma\, g_{MOH}\theta_T}{RT}\right] \tag{6}$$

$$f_{-1} = k_{-1}^{'0}\, \theta_{MOH} \exp\left[\frac{-(1-\beta)\, F\eta}{RT}\right] \exp\left[\frac{(1-\gamma)\, g_{MOH}\theta_T}{RT}\right] \tag{7}$$

Here, similar to β, γ is a symmetry factor between 0 and 1.[12] Assuming the second step as rate determining, Equation (8) can be derived:

$$f_T = f_2 = k_2^{'0}\, \theta_{MOH}\, a_{OH} \exp\left[\frac{\beta F\eta}{RT}\right] \exp\left[\frac{(1-\gamma)\, g_{MOH}\theta_T}{RT}\right] \tag{8}$$

At quasi-equilibrium state, Equation (6) and (7) can be set equal (Equation (9)).

$$\frac{\theta_{MOH}}{\theta_M} \exp\left[\frac{g_{MOH}\theta_T}{RT}\right] = K_1\, a_{OH} \exp\left[\frac{F\eta}{RT}\right] \tag{9}$$

For intermediate coverage values, the ratio of the coverages $\frac{\theta_{MOH}}{\theta_M}$ can be approximated to one. Logarithmized and inserted in (8) gives the following expression (Equation (10)).

$$f_T = k_2^{'0}\, \theta_{MOH}\, a_{OH}^{2-\gamma} K_1^{1-\gamma} \exp\left[\frac{(1+\beta-\gamma)\, F\eta}{RT}\right] \tag{10}$$

From that, the Tafel slope and reaction order can be once again calculated (Equation (11) and (12)).

$$b = \left(\frac{\partial\eta}{\partial \log f_T}\right)_{a_{OH}} = \frac{2.303\, RT}{F\,(1+\beta-\gamma)} \tag{11}$$

$$m = \left(\frac{\partial \ln f_T}{\partial \ln a_{OH}}\right)_{\eta} = 2-\gamma \tag{12}$$

Equation (12) allows rationalizing the reaction orders observed for the lower Tafel region for NiFeC and NiFeB LDH. Indeed, for a reaction order of approx. 1.2, it follows that $\gamma =$ 0.8, and for the corresponding Tafel slope of 72 mV dec^{-1}, $\beta =$ 0.62 follows. For the borate anion, a reaction order of about 1.5 results in $\gamma = 0.5$ and the respective Tafel slope of ca. 60 mV dec^{-1} means $\beta = 0.5$.[12] In particular, the latter result sheds light on why the physisorbed hydrogen peroxide mechanism was chosen to model the OER reaction, as it is the only one capable of rationalizing a Tafel slope of 60 mV dec^{-1} coupled with a reaction order of 1.5.[13] The smaller reaction orders, however, cannot be explained by the second step being rate determining, since γ is smaller than 1. When looking at the proposed mechanism in detail, step (III) can be excluded as the RDS, as deprotonation is likely to be fast in the strong alkaline electrolyte. The fourth step is also unlikely to be rate-determining as the rate constant for this reaction is not potential dependent and the gas formation favors the forward reaction according to the principles of *Le Chatelier*.[8] Therefore, the first step should be taken into account as the RDS. With the quasi equilibrium assumption in mind, the total flux is given by the following equation (Eq. 13).

$$f_T = f_1 = k_1^{'0}\, \theta_M\, a_{OH}^{1-\gamma} K_1^{-\gamma} \exp\left[\frac{(\beta-\gamma)\, F\eta}{RT}\right] \tag{13}$$

From this, the Tafel slope and reaction order can once again be calculated (Eqs. 14 and 15):[8]

$$b = \left(\frac{\partial \eta}{\partial \log f_T}\right)_{a_{OH}} = \frac{2.303\,RT}{F\,(\beta - \gamma)} \quad (14)$$

$$m = \left(\frac{\partial \ln f_T}{\partial \ln a_{OH}}\right)_{\eta} = 1 - \gamma \quad (15)$$

With these assumptions, the other rate determining steps can be justified. For the lower potential behavior of NiFeP LDH, the reaction order of 0.84 corresponds to $\gamma = 0.16$ and the corresponding Tafel slope of 68.5 mV dec^{-1} can be attributed to a β of approx. 1. In the higher potential region, all catalysts show a behavior according to a mechanism where step (I) is RDS, which is in good agreement with Temkin conditions. A symmetry factor of $\gamma = 0.64$ follows for the 0.36 reaction order of the NiFeC LDH, and for the corresponding Tafel slope of 196 mV dec^{-1}, $\beta = 0.94$ follows. In the case of NiFeP LDH, the reaction order of ca. 0.70 can be explained through $\gamma = 0.30$ and the 186 mV dec^{-1} Tafel slope follows with $\beta = 0.62$. Lastly, for the 0.54 reaction order of the NiFeB LDH, $\gamma = 0.46$ and the 148 mV dec^{-1} Tafel slope is obtained with $\beta = 0.86$. Table 2 gives an overview of the rate determining steps of all catalysts in the low and high overpotential region.

Aside from NiFeP LDH, whose entire mechanism appears to be controlled by the very first electron transfer step (I), the other two electrocatalysts have the second electron transfer step (II) as RDS at lower potentials and the first electron transfer step (I) is slowest at higher potentials. This implies the weaker, more difficult adsorption of the hydroxyl anions at higher potentials, which may follow as a result of the increased gas formation at this step. In fact, this gas formation is also how the first step being the RDS for NiFeP LDH at lower potentials can be rationalized: Analyzing the activity curves emphasizes that NiFeP LDH exhibits a lower onset point and overall good activity, which may point towards the earlier gas formation and a subsequent weaker adsorption of the reaction intermediates on the electrode surface. Indeed, the exchange current density is also the smallest for this catalyst, suggesting that its catalytic activity is indeed very good.[28] It must be noted that the dual Tafel behavior in this case is not a result of the change in RDS, but rather caused by the potential-dependent change in coverage of the reaction intermediates under Temkin adsorption conditions.[12]

Another important experimental tool to gain insight into the OER mechanism is electrochemical impedance spectroscopy (EIS). Series of EIS spectra were recorded in a potential range of 0.5–0.7 V (*vs* Ag/AgCl) and are presented in the Nyquist plots in Figure S3. The raw data were fitted according to the Armstrong-Henderson equivalent circuit displayed in Figure 6. Here, R_s is the uncompensated solution resistance and R_{ct} represents the charge transfer resistance. The R_p-C_p loop is of particular importance as it correlates to the relaxation of the surface coverage of an adsorbed intermediate.[8] As proposed by Harrington and Conway, R_p is connected to the production of surface intermediates.[11] The pseudo-capacitance C_p does not have a direct physical meaning, but must appear together with the R_p element in order to properly explain the phase delay.[33] However, for a certain potential range, this element accurately portrays the relaxation of surface coverage of an adsorbed intermediate and can thus be associated with the change in the concentration of charged intermediates at the electrode interface.[10]

Of particular interest is the potential dependence of these different Faradaic elements, as plotted in Figure 7. A noticeable drop of R_{ct} with increasing potential is observed for all catalysts, in good agreement with the better electron transfer kinetics in this region.[10] The much higher resistance for the NiFeC LDH at lower potentials aligns well with its lowered activity, while NiFeP and NiFeB LDHs behave similarly. Upon closer inspection, the borate intercalated LDH appears to have a slightly higher charge transfer resistance at lower potentials and a lower one at higher potentials when compared to NiFeP LDH, which correlates with its previously discussed dual Tafel behavior. More conclusive information can be obtained by analyzing the R_p-C_p loop. Similarly, R_p also decreases with increasing potential, once again implying better overall kinetics at these higher potentials. Noteworthy are the similar resistances of all three catalysts in the higher potential region, which could be explained through the first electron transfer step being the RDS for all researched catalysts under these conditions. At lower potentials, however, NiFeP LDH holds the lowest R_p, supporting its good performance. The potential at which the resistances seem to reach a plateau also correlates with the potential at which the change in Tafel slope occurs, supporting the previous Tafel analysis: The pseudo-capacitance potential dependence plot once again confirms different behavior between the lower and higher potential regions, respectively. However, this is most evident for NiFeP and barely noticeable for NiFeC and NiFeB LDH, emphasizing different charging processes and, consequently, different intermediates in the NiFeP LDH mechanism as compared to the other two catalysts. The noticeably higher

Table 2. Rate determining steps in the low and high Tafel region of the respective intercalated NiFe LDHs.

OP region [mV][a]	RDS[b]		
	NiFeC LDH	NiFeB LDH	NiFeP LDH
275-375	II	II	I
375-475	I	I	I

[a] OP regions picked from the experimental Tafel ranges. [b] Rate determining steps according to the physisorbed hydrogen peroxide mechanism.

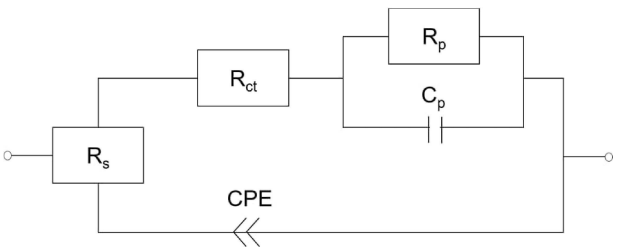

Figure 6. The Armstrong-Henderson equivalent circuit.

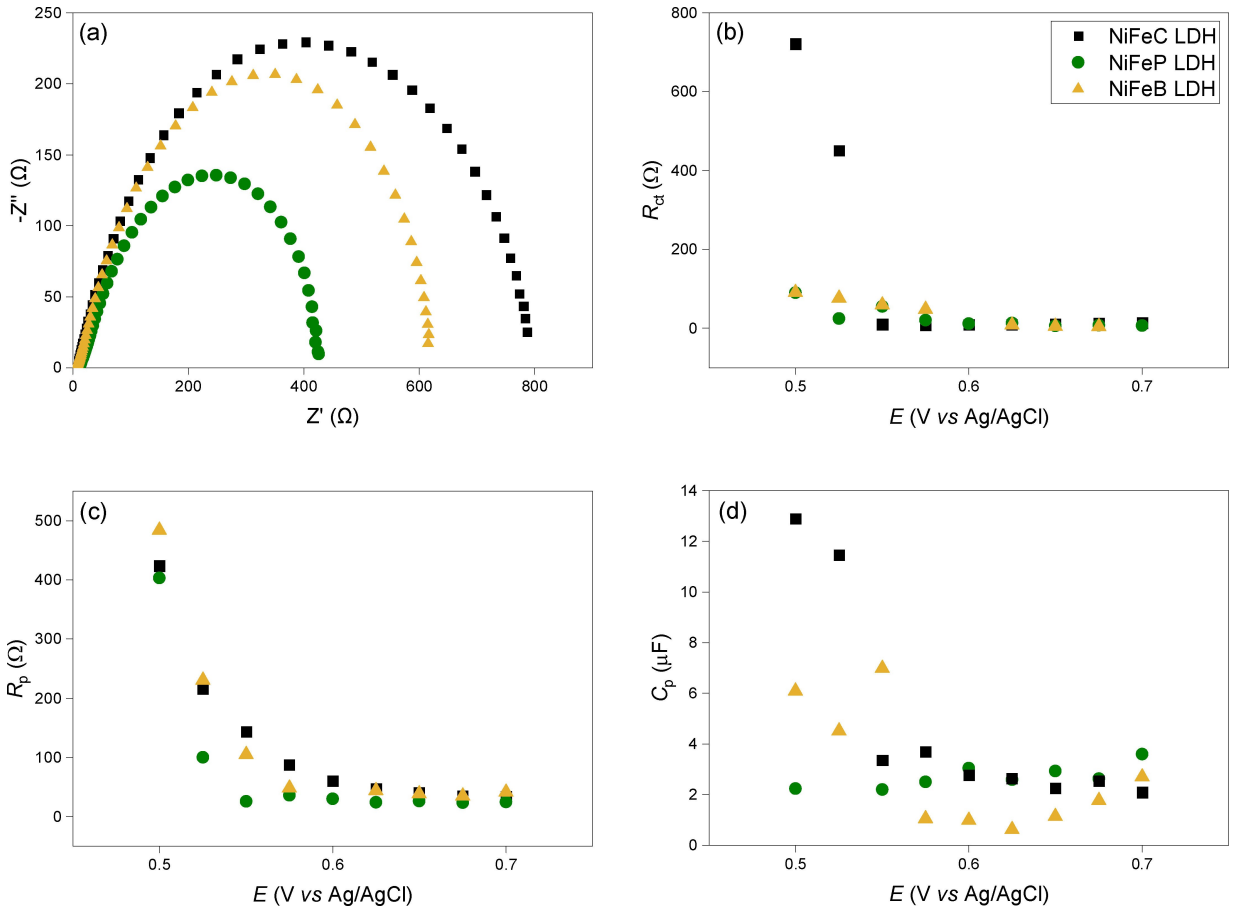

Figure 7. (a) EIS data of NiFeC (black), NiFeP (green) and NiFeB LDH (yellow) at E = 0.5 V *vs* RHE. (b)–(d) Fitting values R_{ct}, R_p and C_p plotted against the applied potential.

capacitances for NiFeP LDH at lower potentials point towards the more sluggish intermediate formation, which is once again in support of the first step being rate determining.

Conclusions

In this work, we have investigated the kinetics and mechanism of NiFe LDH with the intercalated anions carbonate (NiFeC LDH), hypophosphite (NiFeP LDH) and borate (NiFeB LDH). All catalysts showed a dual Tafel behavior and fractional reaction orders whose values could be explained by the model of the physisorbed hydrogen peroxide mechanism and Temkin adsorption conditions. Based on these assumptions, rate limiting steps could be calculated for all three catalysts in both Tafel regions. For NiFeC and NiFeB LDH, the second step (II) was found to be rate determining in the low potential region while the first step (I) is slowest at higher potentials. For NiFeP LDH the entire mechanism appears to be controlled by the first step (I).

Impedance data, that was simulated in terms of the Armstrong-Henderson equivalent circuit, revealed a lowered charge transfer resistance and a lowered rate of surface intermediates formation for NiFeB LDH and NiFeP LDH, explaining the increased activity compared to NiFeC LDH.

Experimental Section

Experimental data available open access: Zenodo 2023, doi.10.5281/zenodo.8031660

Ferric nitrate nonahydrate, sodium carbonate and sodium hydroxide were purchased from Emsure ACS, sodium hypophosphite hydrate and sodium tetraborate decahydrate were purchased from Sigma-Aldrich and nickel nitrate hexahydrate was bought from Alfa Aesar. All reagents were of analytical grade and were used without further purification. Deionized water was used to prepare all reaction solutions. Additionally, for NiFeP and NiFeB LDH DI water was degassed with N_2 to get grid of CO_2.

Typically, NiFeC, NiFeP and NiFeB LDH were synthesized *via* co-precipitation process. First, 16.5 mmol $Ni(NO_3)_2 \cdot 6H_2O$ and 33.0 mmol $Fe(NO_3)_3 \cdot 9H_2O$ were dissolved in 50 mL DI water, forming solution A. Solution B contained 25.0 mmol of the respective anion donating substrate (Na_2CO_3, $NaH_2PO_2 \cdot H_2O$ or $Na_2B_4O_7 \cdot 10H_2O$) and solution A was added dropwise under stirring, forming the precipitated product. To keep the pH value of the reaction solution constant at pH 10, 3.4 M NaOH was prepared and added simultaneously. Once solution A was completely added, the resulting brown dispersion was stirred for another 24 h, before the

product was filtered and washed, until the washing water turned pH 7. The solid was then dried at 80 °C for 12–14 h and finally grinded in a mortar.

Electrochemical studies were performed in a standard three-electrode RDE setup with a glassy carbon rod as the counter electrode (CE) and Ag/AgCl (3 M KCl) as the reference (RE), controlled by a Metrohm Autolab potentiostat PGSTAT302 N. If not mentioned otherwise, 1 M KOH (Chemsolute) solution in Milliq water was used as the electrolyte. For the working electrode, a polished glassy carbon RDE tip was used, which was modified with catalyst ink suspension to obtain a catalyst loading of 0.2 mg cm^{-2}. For catalyst ink, 3 mg of catalyst powder was mixed with 900 μL H_2O and 900 μL EtOH sonicated for 30 min to ensure homogeneity. To obtain a uniform loading, 3×5 μL catalyst ink was dropped onto the RDE tip and dried under a red-light bulb. Lastly, one layer (5 μL) of a 0.1 % Nafion (Sigma Aldrich) was added for catalyst stabilization. For each electrochemical measurement, the electrode was conditioned by running 50 cycles at low scan rates ($\nu = 200$ mV s^{-1}) in order to clean the WE surface.[8] ECSA was measured *via* CV in the region of 0.0–0.1 V at 10 scan rates (0.01, 0.02, 0.04,… 0.18 V s^{-1}). The electrocatalytic activity was also investigated by CV at 0.005 V s^{-1}, whereby only the forward scan was considered. For *iR* correction, EIS was measured after each activity test at 0.5 V from 100 kHz to 100 mHz at the amplitude of 10 mV, to obtain the electrolyte resistance. For impedance series, EIS was further measured at 0.5–0.7 V in 0.025 V steps. For Tafel plots, steady state activity measurements were performed whereby every recorded value was given 150 s to reach equilibrium. For reaction order plots, CV measurements were performed as explained previously in different electrolyte concentrations (0.2–1.0 M KOH in 5 steps).

X-ray diffraction (XRD) patterns were collected on a Bruker D2 Phaser device under CuK_α radiation ($\lambda = 1.54$ Å) with 1° incidence angle and 2θ ranging from 6° to 90° in 0.02° steps. The metal ratio was measured by scanning electron microscopy (SEM, Coxem tabletop EM-30, 1–30 kV) including an energy dispersive X-ray spectroscopy (EDX) detector (Oxford, Bruker). The sample was sputtered beforehand with Au for 1–2 min to increase the conductivity.

Acknowledgements

This work was funded by the Federal Ministry of Education and Research (H2Giga QT1.5 AlFaKat; FKZ 03HY109B). Open Access funding enabled and organized by Projekt DEAL.

Conflict of Interests

The authors declare no conflict of interest.

Data Availability Statement

The data that support the findings of this study are openly available in Zenodo at https://doi.org/10.5281/zenodo.8031660, reference number 8031660.

Keywords: anionic exchange · electrokinetic study · impedance spectroscopy · nickel-iron layered double hydroxides · oxygen evolution reaction

[1] J. Zhao, J.-J. Zhang, Z.-Y. Li, X.-H. Bu, *Small* **2020**, *16*, 2003916.
[2] P. Moriarty, D. Honnery, *Int. J. Hydrogen Energy* **2007**, *32*, 1616.
[3] P. M. Bodhankar, P. B. Sarawade, G. Singh, A. Vinu, D. S. Dhawale, *J. Mater. Chem. A* **2021**, *9*, 3180.
[4] a) Y. Yan, B. Y. Xia, B. Zhao, X. Wang, *J. Mater. Chem. A* **2016**, *4*, 17587; b) C. C. L. McCrory, S. Jung, J. C. Peters, T. F. Jaramillo, *J. Am. Chem. Soc.* **2013**, *135*, 16977.
[5] Z. Lu, W. Xu, W. Zhu, Q. Yang, X. Lei, J. Liu, Y. Li, X. Sun, X. Duan, *Chem. Commun.* **2014**, *50*, 6479.
[6] M. Duan, M. Qiu, S. Sun, X. Guo, Y. Liu, X. Zheng, F. Cao, Q. Kong, J. Zhang, *Appl. Clay Sci.* **2022**, *216*, 106360.
[7] J. A. Carrasco, R. Sanchis-Gual, A. S.-D. Silva, G. Abellán, E. Coronado, *Chem. Mater.* **2019**, *31*, 6798.
[8] L. Negahdar, F. Zeng, S. Palkovits, C. Broicher, R. Palkovits, *ChemElectroChem* **2019**, *6*, 5588.
[9] K. S. Exner, H. Over, *ACS Catal.* **2019**, *9*, 6755.
[10] R. L. Doyle, M. E. G. Lyons, *J. Electrochem. Soc.* **2013**, *160*, H142-H154.
[11] M. E. G. Lyons, M. P. Brandon, *Phys. Chem. Chem. Phys.* **2009**, *11*, 2203.
[12] M. E. G. Lyons, R. L. Doyle, M. P. Brandon, *Phys. Chem. Chem. Phys.* **2011**, *13*, 21530.
[13] M. E. G. Lyons, M. P. Brandon, *Int. J. Electrochem. Sci.* **2008**, *3*, 1425.
[14] a) G. Kreysa, *Electrochim. Acta* **1988**, *33*, 1351; b) A. Damjanovic, A. Dey, J. Bockris, *Electrochim. Acta* **1966**, *11*, 791.
[15] R. F. Scarr, *J. Electrochem. Soc.* **1969**, *116*, 1526.
[16] Y. Matsumoto, E. Sato, *Mater. Chem. Phys.* **1986**, *14*, 397.
[17] J. O. Bockris, T. Otagawa, *J. Electrochem. Soc.* **1984**, *131*, 290.
[18] J. O. Bockris, *J. Chem. Phys.* **1956**, *24*, 817.
[19] M. Luo, Z. Cai, C. Wang, Y. Bi, L. Qian, Y. Hao, L. Li, Y. Kuang, Y. Li, X. Lei, Z. Huo, W. Liu, H. Wang, X. Sun, X. Duan, *Nano Res.* **2017**, *10*, 1732.
[20] D. G. Evans, R. C. T. Slade, in *Layered Double Hydroxides*, Vol. 119 (Eds. X. Duan, D. G. Evans), Springer Berlin Heidelberg, Berlin, Heidelberg, **2006**, pp. 1–87.
[21] A. Flegler, S. Müssig, J. Prieschl, K. Mandel, G. Sextl, *Electrochim. Acta* **2017**, *231*, 216.
[22] S. Sanati, Z. Rezvani, *Ultrason. Sonochem.* **2018**, *48*, 199.
[23] a) W. Zhang, H. Guan, Y. Hu, W. Wang, X. Yang, C. Kuang, *Int. J. Hydrogen Energy* **2022**, *47*, 22731; b) S. Han, S. Liu, S. Yin, L. Chen, Z. He, *Electrochim. Acta* **2016**, *210*, 942.
[24] a) L. Lv, Z. Yang, K. Chen, C. Wang, Y. Xiong, *Adv. Energy Mater.* **2019**, *9*, 1803358; b) Y. Zeng, S. Zhou, *Electrochem. Commun.* **1999**, *1*, 217.
[25] D. Zhou, Z. Cai, Y. Bi, W. Tian, M. Luo, Q. Zhang, Q. Xie, J. Wang, Y. Li, Y. Kuang, X. Duan, M. Bajdich, S. Siahrostami, X. Sun, *Nano Res.* **2018**, *11*, 1358.
[26] J. O. Bockris, A. K. N. Reddy, *Modern Electrochemistry 2B. Electrodics in Chemistry, Engineering, Biology, and Environmental Science*, Kluwer Academic Publishers, Boston, MA, **2004**.
[27] R. Guidelli, R. G. Compton, J. M. Feliu, E. Gileadi, J. Lipkowski, W. Schmickler, S. Trasatti, *Pure Appl. Chem.* **2014**, *86*, 245.
[28] T. Shinagawa, A. T. Garcia-Esparza, K. Takanabe, *Sci. Rep.* **2015**, *5*, 13801.
[29] G. Wu, N. Li, D.-R. Zhou, K. Mitsuo, B.-Q. Xu, *J. Solid State Chem.* **2004**, *177*, 3682.
[30] R. L. Doyle, M. E. G. Lyons, in *Photoelectrochemical solar fuel production. From basic principles to advanced devices* (Eds.: S. Giménez, J. Bisquert), Springer, Switzerland, **2016**, pp. 41–104.
[31] A. A. Mizhir, A. A. Abdulwahid, H. S. Al-Lami, *DWT* **2020**, *202*, 381.
[32] B. E. Conway, M. Salomon, *Electrochim. Acta* **1964**, *9*, 1599.
[33] D. A. Harrington, B. E. Conway, *Electrochim. Acta* **1987**, *32*, 1703.

Manuscript received: May 25, 2023
Revised manuscript received: June 27, 2023
Version of record online: August 9, 2023